A proper motion study of the globular clusters M4, M12, M22, NGC 3201, NGC 6362 and NGC 6752 [*]

K. Z l o c z e w s k i[1], J. K a l u z n y[1], M. R o z y c z k a[1],
W. K r z e m i n s k i[1], B. M a z u r[1],
and I. B. T h o m p s o n[2]

[1]Nicolaus Copernicus Astronomical Center, ul. Bartycka 18, 00-716 Warsaw, Poland
e-mail: (kzlocz, jka, mnr, wk, batka)@camk.edu.pl
[2]The Observatories of the Carnegie Institution of Washington, 813 Santa Barbara Street, Pasadena, CA 91101, USA
e-mail: ian@obs.carnegiescience.edu

ABSTRACT

We derive relative proper motions of stars in the fields of globular clusters M4, M12, M22, NGC 3201, NGC 6362 and NGC 6752 based on a uniform data set collected between 1997 and 2008. We assign a membership class for each star with a measured proper motion, and show that these membership classes can be successfully used to eliminate field stars from color-magnitude diagrams of the clusters. They also allow for the efficient selection of rare objects such as blue/yellow/red stragglers and stars from the asymptotic giant branch. Tables with proper motions and photometry of over 87000 stars are made publicly available via the Internet.

Key words: *globular clusters: individual: M4, M12, M22, NGC 3201, NGC 6362, NGC 6752 – astrometry – blue stragglers*

1   Introduction

Globular clusters (GCs) offer an excellent opportunity to study the chemical evolution of the universe, to test the theory of stellar evolution, and to assess the quality and accuracy of numerical codes written to follow the dynamical evolution of multi-body systems. To fully exploit this opportunity, cluster members must be discerned from field stars, which can be achieved e.g. by a proper motion (PM) study. As emphasized by Bellini, Anderson and van der Marel (2012), such studies impose strong constraints on structure, dynamics and evolution of GCs. They also allow the identification of cluster members occupying unusual locations in the H-R diagram (e.g. blue, yellow and red stragglers), and, when supplemented with additional data, a measurement of absolute motions and geometric distances of GCs.

The first PM studies of GCs date from the 1970's. However the statistical uncertainties were often larger than the internal velocity dispersion (**?**, and references therein). The breakthrough came with the advent of CCD detectors and the launch of the Hubble Space Telescope. Extensive HST-studies of numerous GCs have been undertaken, most of which are not yet finished (**?**). To our knowledge, just two large catalogs of PMs derived from Hubble data are accessible online as of today: 47 Tuc (**?**) and ω Cen (**?**). A valuable extension of the latter is the catalog compiled by **?** using ESO archive CCD data.

---

[*]Based on data obtained at the Las Campanas Observatory.

Table 1: Equatorial coordinates of field centers.

Field	α_{2000} [deg]	δ_{2000} [deg]
M4-F1	245.89492	-26.52768
M4-F2	245.90846	-26.58710
M12	251.81906	-1.95024
M22	279.10275	-23.90205
NGC 3201-F1	154.40702	-46.40682
NGC 3201-F2	154.37700	-46.39437
NGC 6362	262.98281	-67.04611
NGC 6752	287.72575	-59.97099

As **?** show, ground-based CCD observations with temporal baselines of 4 years are sufficient to reliably separate members of nearby clusters from field stars. Similar conclusions have been reached by **?** for the globular clusters M4 and NGC 6397, **?** for the open cluster M67, and **?** for the open cluster NGC 6253.

More recently Zloczewski, Kaluzny & Thompson (2011) published a PM catalog for M55 based on CCD observations performed at the Las Campanas Observatory (LCO) between 1997 and 2008. In the present paper we derive relative PMs for another six GCs: M4, M12, M22, NGC 3201, NGC 6362 and NGC 6752. In Sec. 2 we describe the observational data and methods used to prepare the CCD images for the analysis. The procedures employed for the determination of relative PMs of individual stars are discussed in Sec. 3. Color-magnitude diagrams (CMD) of individual clusters, cleaned from field stars, are presented in Sec. 4 followed by a brief Summary.

2   Data selection and preparation

The images analyzed in this paper are a part of the data collected between 1997 and 2008 within the CASE project (Cluster AgeS Experiment; see **?**). All observations were made with the 2.5-m du Pont telescope at LCO using the same detector and the same set of V and I filters. We used the TEK5 CCD camera with a field of view of 530×530 arcsec and a scale of 0.259 arcsec/pixel. We observed two fields for M4, two for NGC 3201 and one for each of the remaining four clusters. Equatorial coordinates of the centers of the analyzed fields are listed in Table **??**. For each cluster and each observing run we selected a collection of V-frames obtained at an air-mass less than 1.1 and a seeing better than 1.1 arcsec, henceforth referred to as a *data set*. Frames obtained through cirrus, as well as those with a bright background, were rejected. Altogether we collected 42, 24, 15, 33, 27 and 22 data sets for M4, M12, M22, NGC 3201, NGC 6362 and NGC 6752, respectively. For each data set we constructed an *averaged frame* with a high signal-to-noise ratio using the Difference Image Analysis PL (DIAPL) package[†] developed by Wojtek Pych. The construction procedure consisted of the following steps:

1. Find the frame with the best seeing (henceforth *the reference frame*).

2. Transform the remaining frames to the coordinates of the reference frame (bicubic spline interpolation was used).

[†]Freely available at http://users.camk.edu.pl/pych/DIAPL/

3. Find the point spread function (PSF) of each frame and transform it to match that of the reference frame.

4. Stack the transformed images.

To reduce the effects of PSF variability, the reference frame as well as individual frames were divided into 16 overlapping subframes, and the procedure was applied to each subframe separately.

Next, a *master list* of stars was compiled for each cluster based on the best averaged frame of that cluster (henceforth *master frame*). To that end the master frame was divided into 16 subframes, and the DAOPHOT/ALLSTAR package (**?**) was run for each subframe, assuming a Moffat function with linear spatial variability to characterize the PSF. Because of crowding the compilation proceeded in an iterative way, gradually decreasing the detection threshold. We took care to avoid artificial splitting of bright stars which can happen when an automatic procedure is used to detect missed objects in subtracted images. During the final iteration the residual images were inspected by eye to find previously undetected objects.

The listed stars were subsequently identified in the remaining averaged frames of a given cluster, and profile photometry as well as PSF modeling was performed for those frames with the ALLSTAR parameter *REDET* set to 1, i.e. allowing for the re-determination of coordinates.

3   Proper motions

To derive the PMs we employed the same method as **?**. For convenience, we briefly review the method in this section.

3.1   Measurements

In each averaged frame of a given cluster the position of each star from the master list was determined with respect to nearby cluster members using a procedure similar to that described by **?**. For the first guess we defined cluster members as objects located on the main sequence, red giant branch and horizontal branch of the CMD of the cluster. To select them from the master list a $V/(V-I)$ or $V/(B-V)$ CMD was constructed, composed of stars with $V < 21.0$ mag and good photometry. The photometric quality was evaluated based on fit parameters CHI and $SHARP$ returned by ALLSTAR: stars with $0.02 < CHI < 1.00$ and $-0.3 < SHARP < 0.3$ were only included.

Next, to each star a set of *grid objects* was assigned, composed of cluster members located in an $\sim80\times80$ arcsec square centered on that star. The grid objects were used to define the local geometrical transformation between the master frame and the averaged frame being processed. Typically, there were ~200 of them per star. For the transformation function a two-dimensional 3rd order Chebyshev polynomial was chosen, whose parameters were calculated with the help of IRAF[‡] tasks immatch.geomap and immatch.geoxytran.

The (X_0, Y_0) coordinates of the star on the master frame were transformed into the expected coordinates (X_C, Y_C) on the averaged frame, and relative motions $dX = X_C - X_0$ and $dY = Y_C - Y_0$ were calculated. Finally, using relative motions from all suitable averaged frames, the PMs of the star μ_X and μ_Y

[‡]IRAF is distributed by the National Optical Astronomy Observatories, which are operated by the AURA, Inc., under cooperative agreement with the NSF.

were obtained from linear least-square fits to dX and dY as functions of time. The fitting was only attempted for objects with positions determined in at least four epochs spanning at least four years. The confidence level was set to 99%, i.e. all stars for which the significance of the fit was smaller than 99% were rejected. Grid stars for which reliable PMs had been obtained were then shifted to positions corresponding to the epoch at which the reference frame was taken. Transformations and fits were then repeated. The final total PMss were calculated from the standard formula $\mu = (\mu_X^2 + \mu_Y^2)^{1/2}$.

The catalog of the derived PMs, whose first few lines are shown in Table **??**, is available online at http://case.camk.edu.pl. Altogether it contains data for 13037, 12655, 10962, 22545, 11782 and 12987 stars in M4, M12, M22, NGC 3201, NGC 6362 and NGC 6752, respectively Equatorial coordinates of the stars were obtained using frame astrometric solutions based on a set of stars with $V < 17$ selected from the UCAC3 catalog (**?**). The average residual of the adopted solution varied between 0.15 arcsec for NGC 6362 and 0.21 arcsec for M4.

3.2 Error estimates

In the overlapping part of the two fields containing M4 (NGC 3201) there were 10385 (17693) stars with measured PMs. For 66 per cent of them the difference between PMs measured in each field separately was smaller than 0.16 (0.08) mas/yr, which can be adopted as a robust estimate of the average error of the PM determination. For 95 per cent of the stars the difference was smaller than 0.75 (0.37) mas/yr. The median differences were nearly the same in all magnitude ranges.

The formal error σ_μ of the total proper motion was derived for each star from the least-square fit described in Sect. **??**. For stars with $V \approx 19.0$ the median value of σ_μ varied from 0.29 to 0.67 mas/yr (observed in NGC 3201 and M4, respectively). Not surprisingly, these limits were increasing for fainter stars, and at $V \approx 20$ they reached 0.46 and 1.62 mas/yr (observed, respectively, in NGC 3201 and NGC 6362). An increasing scatter in σ_μ was also observed in all clusters for $V < 14.5$. This is due to the saturation of bright stars on some images, resulting in fewer averaged frames available for the PM measurement. In general, we may say that for $V < 17.0$ the formal PM errors result mainly from systematic effects, while at fainter magnitudes their main source is photon noise.

Table 2: First few lines of the PM catalog for M4. Columns: (1) star ID (starting with 1 and 2 for fields F1 and F2, respectively); (2) & (3) equatorial coordinates $(\alpha, \delta)_{2000.0}$ for epochs 1995.41 and 2008.45 for F1 and F2, respectively; (4) & (5) XY pixel coordinates on reference frames; (6)–(9) PMs and their errors; (10) number of epochs used; (11) temporal baseline; (12) cluster membership (for explanation see Sec. 3.4); (13) V magnitude (obtained from an approximate transformation performed for all stars) (14) V magnitude (obtained from an accurate transfromation, olny performed for stars with known colors); (14) V ; (15) error of V; (16) B-V ; (17) error of B-V. The whole catalog is available online at case.camk.edu.pl.

ID	α	δ	X	Y	$\mu_\alpha \cos\delta$	$\sigma_{\mu_\alpha \cos\delta}$	μ_δ	σ_{μ_δ}	N	dT	mem	V	V	σ_V	$B-V$	σ_{B-V}
(1)	(2)	(3)	(4)	(5)	(6)	(7)	(8)	(9)	(10)	(11)	(12)	(13)	(14)	(15)	(16)	(17)
[#]	[°]	[°]	[pixel]	[pixel]	[mas/yr]	[mas/yr]	[mas/yr]	[mas/yr]	[#]	[yr]	[-]	[mag]	[mag]	[mag]	[mag]	[mag]
1110412	245.975229	-26.575613	354.062	20.026	-0.19	0.31	-1.09	0.87	6	5.086	2	20.468	20.467	0.027	1.332	0.026
1110303	245.973278	-26.589989	155.339	43.471	-1.40	0.82	0.19	0.64	8	11.076	2	19.389	19.385	0.008	1.069	0.012
1110429	245.972717	-26.582292	261.684	50.800	0.12	0.97	-0.14	0.38	19	14.081	2	20.584	20.586	0.028	1.507	0.023
1110294	245.971364	-26.570567	423.667	68.152	10.86	1.08	12.26	0.39	26	14.081	0	19.332	19.332	0.010	1.337	0.018
1110124	245.969529	-26.593671	104.340	89.706	-0.12	0.24	-0.31	0.26	8	11.076	2	17.849	17.842	0.004	0.847	0.009
1110150	245.969449	-26.574499	369.270	91.668	8.35	0.31	14.72	0.12	8	11.076	0	18.142	18.139	0.004	1.135	0.010
1110197	245.969333	-26.582213	262.658	92.719	-0.05	0.36	-0.04	0.35	8	11.076	2	18.533	18.527	0.004	0.909	0.010
1110454	245.969287	-26.587998	182.719	93.000	0.47	1.14	1.07	1.03	27	14.081	2	20.850	20.851	0.033	1.491	0.034
1116026	245.969344	-26.564876	502.233	93.448	1.11	1.08	1.73	1.67	36	14.081	0	21.057	21.059	0.047	1.515	0.057
1110450	245.969205	-26.566927	473.888	95.064	-3.33	1.13	-1.86	1.26	11	11.072	0	20.836	20.836	0.030	1.423	0.025
1110364	245.968586	-26.573083	388.804	102.426	0.62	0.67	-0.65	0.80	8	11.076	2	19.995	19.994	0.013	1.294	0.016
1110460	245.967451	-26.596180	69.589	115.308	0.33	1.50	0.10	0.74	25	14.081	2	20.934	20.936	0.033	1.512	0.029
1110230	245.966177	-26.579653	297.929	131.927	0.52	0.31	0.31	0.57	8	11.076	2	18.816	18.811	0.006	0.987	0.011
1116023	245.964502	-26.581214	276.299	152.590	-0.48	0.46	-0.74	0.30	8	11.076	2	18.487	18.482	0.010	0.943	0.020
1110417	245.963061	-26.564212	511.200	171.276	-0.91	0.87	1.34	1.22	12	11.072	2	20.495	20.497	0.023	1.543	0.025
1110240	245.962554	-26.574815	364.663	177.022	6.59	0.77	19.90	0.68	8	11.076	0	18.921	18.922	0.026	1.410	0.039
1110411	245.962965	-26.565007	500.205	172.428	7.49	0.60	13.13	0.78	12	11.072	0	20.464	20.457	0.013	0.839	0.022
1110355	245.962111	-26.572929	390.700	182.599	-1.06	0.62	-0.00	0.34	8	11.072	2	19.896	19.894	0.012	1.227	0.017
1116024	245.961945	-26.573605	381.363	184.615	-1.34	0.84	0.52	0.72	8	11.076	2	19.998	19.996	0.015	1.292	0.024
1110389	245.962454	-26.598838	32.689	177.032	0.72	0.88	1.00	0.84	25	14.081	2	20.189	20.188	0.019	1.295	0.020
1110327	245.960497	-26.569715	435.069	202.742	-0.07	0.41	0.94	0.77	10	11.076	2	19.617	19.614	0.008	1.148	0.015
1110127	245.959694	-26.598007	44.089	211.241	-0.44	0.22	-0.37	0.42	7	5.087	2	17.906	17.899	0.004	0.833	0.013
1110288	245.958568	-26.571603	408.911	226.518	-0.96	0.42	1.28	0.21	8	11.076	2	19.284	19.279	0.008	1.068	0.012
1110299	245.956955	-26.579173	304.249	246.098	9.64	0.37	15.23	0.40	8	11.076	0	19.366	19.362	0.009	1.119	0.013
1110298	245.956527	-26.574304	371.513	251.637	-0.91	0.44	-0.38	0.69	8	11.072	2	19.360	19.356	0.009	1.123	0.014
1110418	245.955256	-26.568132	456.756	267.677	-0.12	1.11	1.26	1.04	35	14.081	2	20.501	20.503	0.030	1.516	0.025
1110238	245.954365	-26.578801	309.290	278.163	-1.15	0.61	0.49	0.47	8	11.076	2	18.909	18.904	0.006	1.006	0.011
1110198	245.953445	-26.594167	96.936	288.752	1.25	0.35	0.09	0.33	8	11.076	2	18.537	18.531	0.005	0.905	0.014

Table 3: Number of stars belonging to membership classes 0, 1 and 2.

Cluster	0	1	2
M4	2229	174	10633
M12	1477	38	11139
M22	2476	28	8457
NGC 3201	3225	237	19082
NGC 6362	1948	124	9709
NGC 6752	1015	129	15250

3.3 Completeness

We defined the completeness of our survey as the ratio of the number of stars for which the PM was successfully measured to the number of stars for which the PM measurement was attempted, and we assessed it as a function of V-magnitude and radial distance from the center of the cluster r. In most clusters the completeness exceeds $\sim$70 per cent for $13 < V < 17$ and drops to ~ 25 per cent at $V = 20.0$. The exception is M22, where it is limited to $\sim$50 per cent, which is understandable given heavy crowding of the field. As expected, the completeness increases with r, flattening at about 4 arcmin. The drop observed at small r is due to crowding, and the similar drop at large distances - due to the fact that for more distant stars only a few epochs were often available. No attempt was made to estimate the completeness of master lists. As it is for other ground based studies, this parameter is a strong function of the distance from the cluster center.

3.4 Cluster membership

Vector point diagrams (VPD) showing stars with reliable PMs are presented in Figs. **??** – **??**. In all six cases cluster members are crowded around the (0,0) point, and it is evident that field stars are a small fraction of the total sample. For the clusters M4, M22 and NGC 3201 field stars form well defined clumps on the VPD that barely overlap with the cluster stars. For the remaining three clusters field stars do not show well defined clumps on the VPD. Instead they are spread over large areas on the VPD and their distribution overlaps with cluster stars. These properties of the VPDs and the small percentage of field stars in the analyzed samples prevented us from estimating membership probabilities as it is usually done (see e.g. **?**). Instead, we assigned each star to one of three membership classes ($mem = 0,1,2$) based on its location in the VPD and the error σ_μ. Class 0 corresponds to likely field stars, class 1 to possible members and class 2 to likely members. The assignment procedure consisted of the following steps:

1. All stars were divided into magnitude bins containing at least $\sim$1000 objects.

2. In each bin mean values (M_α, M_δ) and standard deviations (S_α, S_δ) of the distributions of PM components in α and δ directions were found. The total standard deviation $S \equiv (S_\alpha^2 + S_\delta^2)^{1/2}$ was calculated.

3. In each bin mean values (ME_α, ME_δ) and standard deviations (SE_α, SE_δ) of the distributions of the errors of PM components in α and δ directions were found. Total mean error $ME \equiv (ME\alpha^2 + ME_\delta^2)^{1/2}$ and total standard deviation of the error $SE = (SE\alpha^2 + SE_\delta^2)^{1/2}$ were calculated.

4. Stars with $\mu > aS$, where a was equal to 2.5 for M4 M22 and NGC 3201, and to 2.0 for M12, NGC 6362 and NGC 6752, were classified as nonmembers ($mem = 0$). Stars with $\mu \leq aS$ and $\sigma_\mu > ME + aSE$ were classified as possible members ($mem = 1$), while those with $\mu \leq aS$ and $\sigma_\mu \leq ME + aSE$ as genuine PM-members of the cluster ($mem = 2$).

The histograms showing the distributions of both PM components for the brightest and for the faintest bin in V are shown in Figs. **??** – **??** together with the corresponding VPDs. Table **??** lists the number of stars assigned to membership classes 0, 1 and 2 for each cluster.

4   Color-magnitude diagrams

Figures **??** – **??** show CMDs of the six analyzed cluster fields. The photometry of M12, M22 and NGC 3201 was calibrated using local standards from **?** catalog. For M4, NGC 6362 and NGC 6752 the calibration was based on observations of **?** standards collected within CASE with instrumentation described in Sec. 2. Left panels of Figs. **??** – **??** include all stars with measured proper motion and with good photometry. Poor photometric measurements were filtered out by identifying stars with relatively large formal error of magnitude or color as compared with other stars of similar magnitude. Middle panels include only likely cluster members ($mem = 2$). Right panels show a zoomed view of the turnoff region with the location of known variables identified. As for the middle panels, only stars with $mem = 2$ are plotted. Lists of variable stars were taken from published and unpublished CASE surveys.

Comments on individual clusters:

M4 – In addition to about two dozen blue straggler stars, panel B of Fig. **??** shows about a dozen candidate yellow straggler stars. Only one of the blue stragglers is a known variable. Several likely cluster members are observed to the blue of the main sequence below turnoff region. One of those faint blue stars is the binary hot subdwarf V46 (**??**).

M12 – This cluster shows about two dozen candidates for blue and yellow stragglers (Fig. **??** B, C). Nine of them were identified as variables. A few likely members are observed to the red of the turnoff, and one is observed to the red of the subgiant branch. These are potentially interesting objects, deserving spectroscopic follow-up.

M22 – This cluster is located in front of the outer part of the Galactic bulge. Comparison of panels A and B in Fig. **??** shows that field interlopers have been efficiently filtered out. Relatively few candidates for blue stragglers, as compared with M4 and M12, are observed in panels B and C. The relatively large widths of the subgiant and giant branches results from a combination of differential reddening and chemical inhomogeneity of the cluster (**?**). One may also notice that the extended horizontal branch of M22 exhibits at least three gaps on the CMD. The pronounced gap at $V = 14.6$ has been reported earlier by **?** but is more clearly seen in our data. Two other possible gaps are located at $V \approx 16$ and $V \approx 17$. Most of the variables reported so far by CASE for the central region of M22 turned out to be field stars (**??**).

NGC 3201 – Like M22, this cluster suffers from differential reddening causing a large width of the principal features of the CMD (**?**). As is apparent in panels B and C of Fig. **??**, the cluster hosts a rich population of blue and yellow stragglers (note, however, that stars observed at $V < 16$ and $B-V < 0.4$ belong to the blue horizontal branch). Several blue stragglers are SX Phe type pulsating variables (**?**). One hot subdwarf candidate is seen at $V = 19.2$ and $V-I = -0.01$.

NGC 6362 – As we noted in Sect. **??**, cluster members overlap with field objects on the VPD (see Fig. **??**). Therefore, some likely interlopers can still remain in panels B and C of Fig. **??**. Nonetheless, it is evident that the cluster hosts a rich population of blue and yellow stragglers. The variable hot subdwarf identified by **?** is a likely cluster member. In Fig. **??** this stars is located at $V = 19.09$ and $B-V = -0.23$. A pronounced asymptotic giant branch is clearly visible in the CMD.

NGC 6752 – Several stars are located to the red of the subgiant branch and main-sequence in panel B of Fig. **??**. The poor separation of cluster stars from field stars on the VPD (see Fig. **??**) suggests that these may be field interlopers not recognized by our simple membership criteria. Spectroscopic observations are needed to clarify status of these stars. On the other hand, a large fraction of the variables identified by **?** are likely cluster members.

5   Summary

Based on a uniform set of data collected between 1997 and 2008 we derived relative proper motions of stars in the fields of six globular clusters: M4, M12, M22, NGC 3201, NGC 6362 and NGC 6752. The measurements were made using a procedure similar to that described by **?**. Proper motions were successfully measured for over 87000 stars and a membership class was assigned to each. The membership classes allow for an efficient elimination of field stars from color-magnitude diagrams of the clusters. A catalog of proper motions was compiled and is publicly available at case.camk.edu.pl. These relative proper motions aid in the efficient selection of rare objects such as blue/yellow/red stragglers and stars from the asymptotic giant branch. The data can be also used to assign membership status to variable stars, either already identified or to be detected by future surveys.

Acknowledgments

References

Anderson, J., Bedin, L. R., Piotto, G., Yadav, R. S., and Bellini, A. 2006, A&A, 454, 1029

Anderson J., and van der Marel R. P. 2010, ApJ, 710, 1032

Bellini, A., Piotto, G., Bedin, L. R., Anderson, J., Platais, I., Momany, Y., Moretti, A., Milone, A. P., and Ortolani, S. 2009, A&A, 493, 959

Bellini A., Anderson J., and van der Marel, R. 2012, HST proper motions of globular clusters, available at http://mpia.de/ dynamics/ringberg/?view=program in online proceedings of "Dynamics meets kinematic tracers" conference held on April 10–14, 2012 at Ringberg Castle

Clement Ch. M. *et al.* 2001, AJ, 122, 2587

Cudworth K. M. 1980, IAU Symp. No. 85, p.431

Dinescu D. I., van Altena W. F., Girard T. M., and Lopez, C. E. 1999, AJ, 117, 277

Dinescu D. I., Girard, T. M., van Altena, W. F., and Lopez, C. E. 2005, ApJ, 618L, 25

Harris, W. E. 1996, AJ, 112, 1487

Girard, T. M., Grundy, W. M., Lopez, C. E., and van Altena, W. F. 1989, AJ, 98, 227

Cho, D. H., Lee, S-W, Sung, H. 1989, JKAS, 31, 67

Ibata R. A., Gilmore G. F., and Irwin M. J. 1994, Nature 370, 194

Ibata R. A., Wyse R. F. G., and Gilmore G. F., Irwin M. J., Suntzeff, N. B. 1997, AJ 113, 634

Kaluzny, J., Thompson, I. B., and Krzeminski, W. 1997, 113, 2219

Kaluzny, J., and Thompson, I. B. 2001, A&A, 373, 899

Kaluzny, J. *et al.* 2005, AIPC (eds. J.Mikolajewska, A.Olech), 752, 70

Kaluzny, J., Pietrukowicz, P., Thompson, I. B., Krzeminski, W., Schwarzenberg-Czerny, A., Pych, W., and Stachowski, G. 2005, MNRAS, 359, 677

Kaluzny, J., and Thompson, I.B. 2009, Acta Astronomica, 59, 273

Kaluzny, J., Thompson, I.B., Krzeminski, W., and Zloczewski, K. 2010, Acta Astronomica, 60, 245

Landolt, A. U. 1992, AJ, 104, 340

Lanzoni, B., Dalessandro, E., Perina, S., Ferraro, F. R., Rood, R. T., and Sollima, A. 2007, ApJ, 670, 1065

Majewski S., Skutskie, M. F., Weinberg, M. D., and Ostheimer J. C. 2003, ApJ, 599, 1082

Marino, A. F. 2011, A&A, 532, 8

Mazur, B., Kaluzny, J., and Krzeminski, W. 1999, MNRAS, 306, 727

Mazur, B., Krzeminski, W., and Thompson, I. B. 2003, MNRAS, 340, 1205

McLaughlin D. E., Anderson J., Meylan G., Gebhardt K., Pryor C., Minniti D., Phinney S. 2006, ApJS, 599, 1082

Montalto, M., Piotto, G., Desidera, S., Platais, I. Carraro, G., Momany, Y., de Marchi, F., and Recio-Blanco, A. 2009, A&A, 505, 1129

Olech, A., Kaluzny, J., Thompson, I. B., Pych, W., Krzeminski, W., and Schwarzenberg-Czerny, A. 1999, AJ, 118, 442O

O'Toole, S. J., *et al*. 2006, Baltic Astronomy, 15, 61

Peng, C. Y., Ho, L. C., Impey, C. D., and Rix, H.-W. 2010, AJ, 139, 2097

Pietrukowicz, P., and Kaluzny, J. 2003, AcA, 53, 371

Platais, I., Kozhurina-Platais, V., Mathieu, R. D., Girard, T. M., and van Altena, W. F. 2003, AJ, 126, 2922

Pryor, C., Piatek, S., and Olszewski, E. W. 2010, AJ, 139, 839

Pych, W., Kaluzny, J., Krzeminski, W., Schwarzenberg-Czerny, A., and Thompson, I. B. 2001, A&A, 367, 148

Sollima, A., Beccari, G., Ferraro, F. R., Fusi Pecci, F., and Sarajedini, A. 2007, MNRAS, 380, 781

Stetson, P. B. 2000, PASP, 112, 925

Stetson, P. B. 1987, PASP, 99, 191

von Braun, K., and Mateo, M. 2001, AJ, 121, 1522

Yadav, R. K. S. *et al*. 2008, A&A, 484, 609

Zacharias, N. *et al*. 2010, AJ, 139, 2184

Zloczewski K., Kaluzny J., and Thompson I. B. 2011, MNRAS, 414, 3711
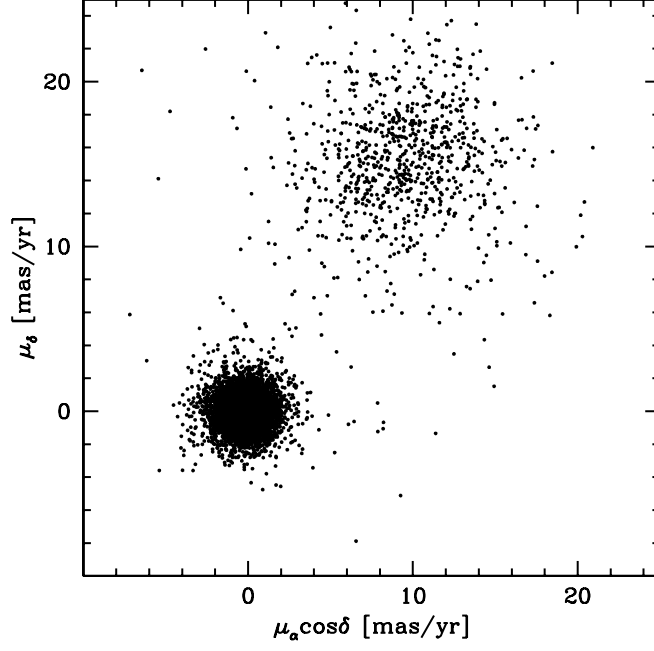
Figure 1: Results for M4. Vector point diagram for 13038 stars with measured relative proper motions.
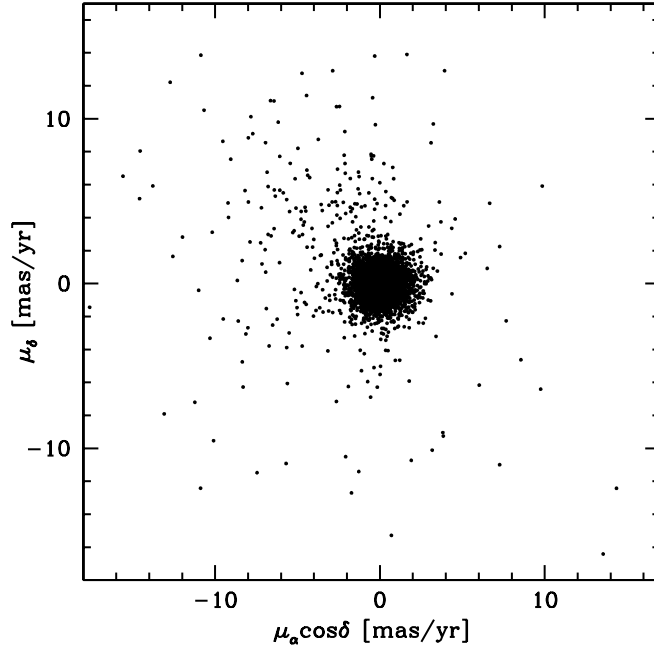
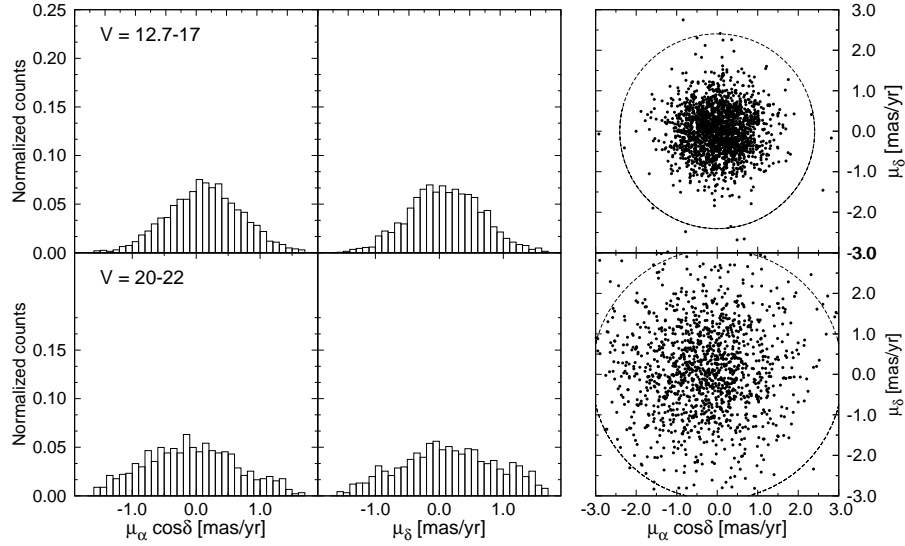Figure 2: Results for M12. Vector point diagram for 12654 stars with measured relative proper motions.
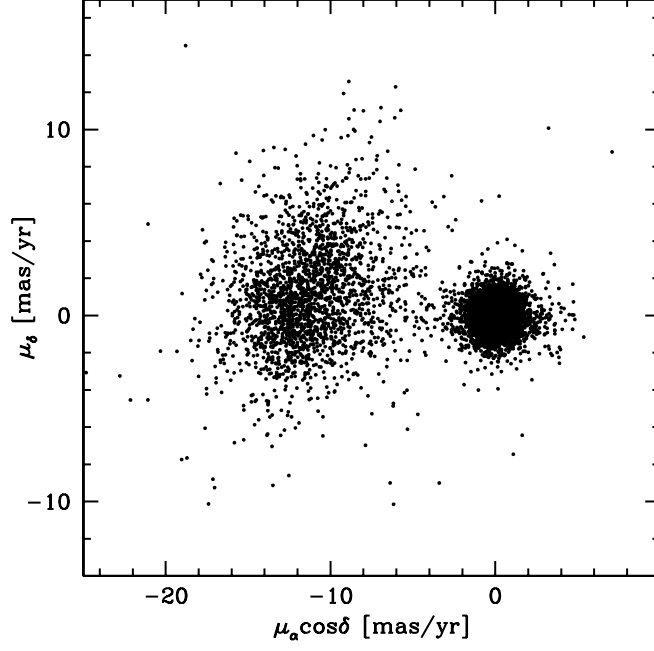
Figure 3: Results for M22. Vector point diagram for 10961 stars with measured relative proper motions.
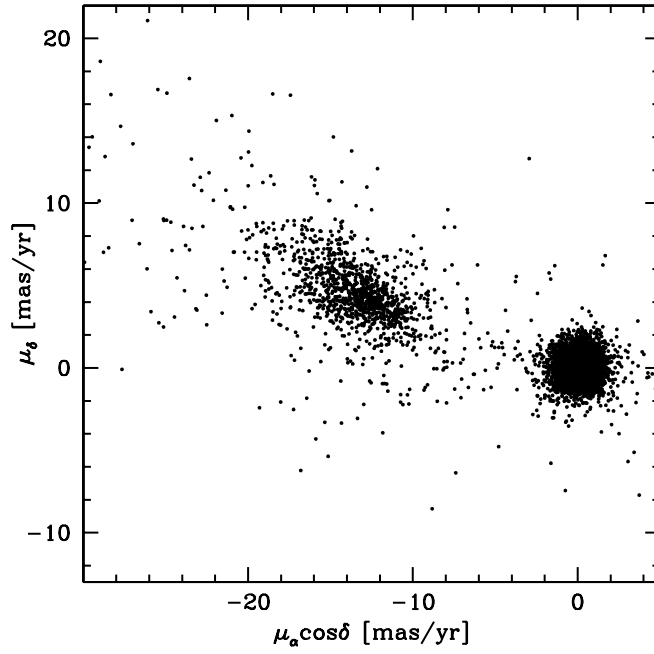
Figure 4: Results for NGC 3201. Vector point diagram for 22544 stars with measured relative proper motions.
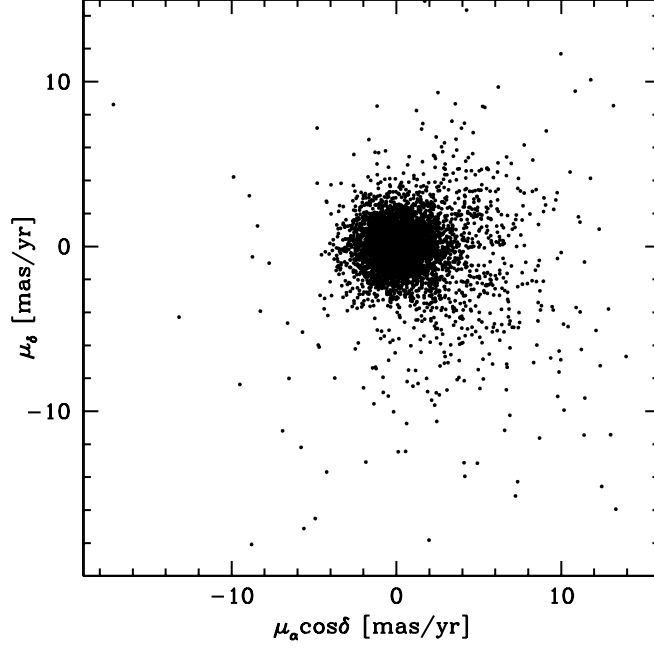
Figure 5: Results for NGC 6362. Vector point diagram for 11788 stars with measured relative proper motions.
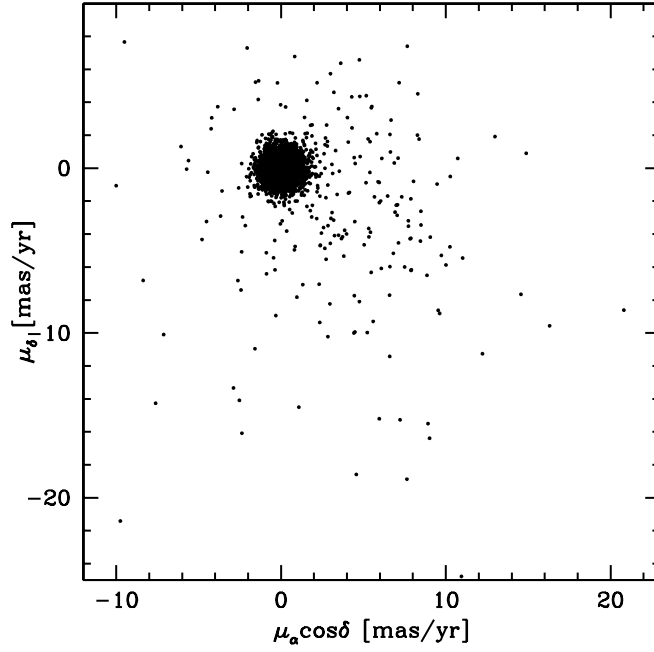
Figure 6: Results for NGC 6752. Vector point diagram for 12986 stars with measured proper motion.
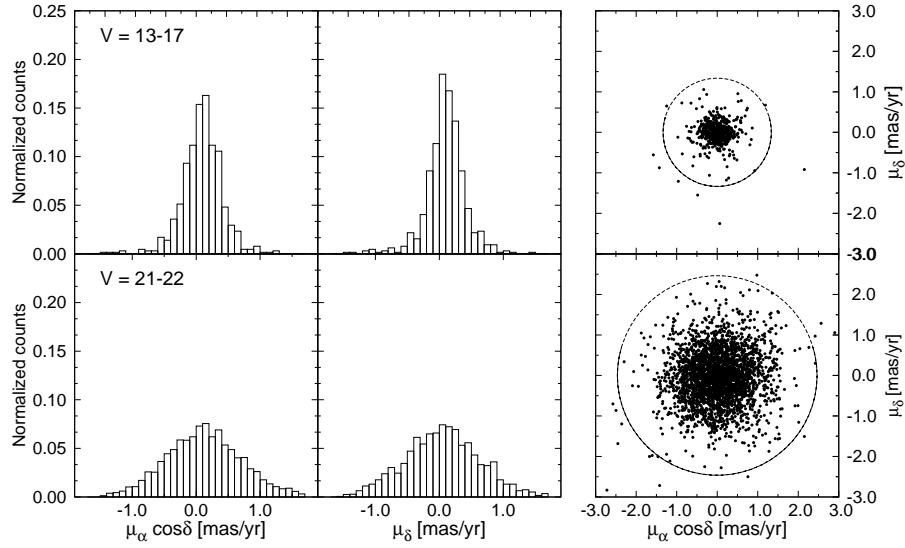
Figure 7: Results for M4. Distributions of $\mu_\alpha \cos\delta$ and μ_δ in bins $V = 12.7 - 17$ and $V = 20 - 22$ mag (left), and the corresponding vector point diagrams (right). The radii of the circles in the right panel are equal to $3S$ with $S = 0.80$ and 1.03 mas yr^{-1} in upper and lower diagram, respectively.
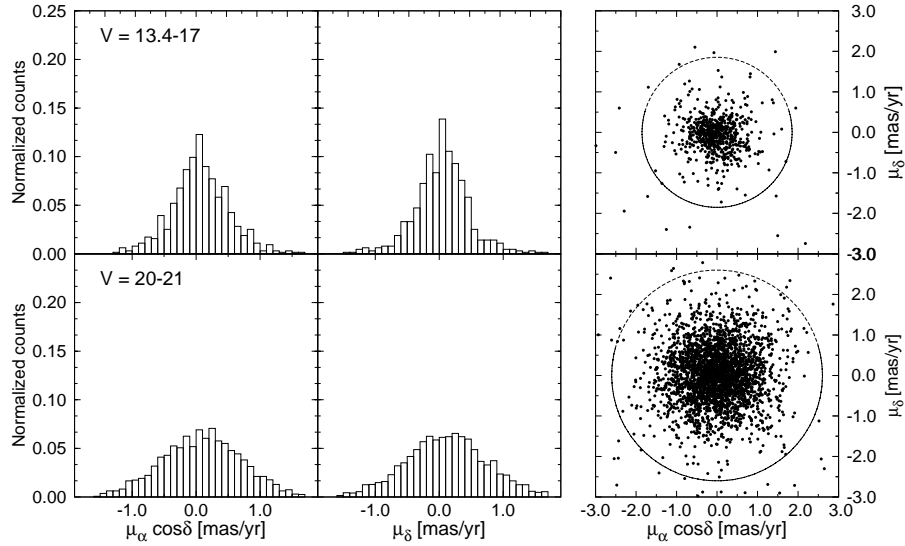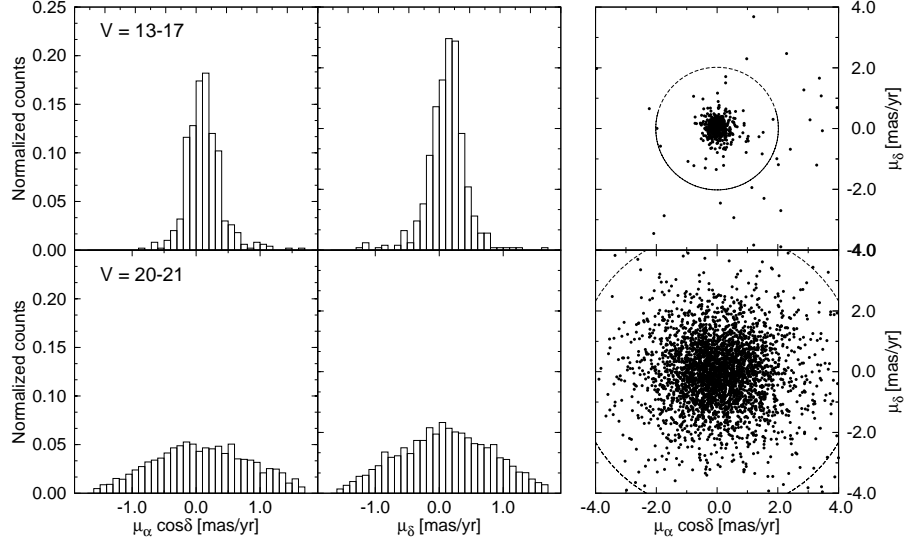

Figure 8: Results for M12. Distributions of $\mu_\alpha \cos\delta$ and μ_δ in bins $V = 13.4 - 17$ and $V = 20 - 21$ mag (left), and the corresponding vector point diagrams (right). The radii of the circles in the right panel are equal to $3S$ with $S = 0.62$ and 0.87 mas yr^{-1} in upper and lower diagram, respectively.
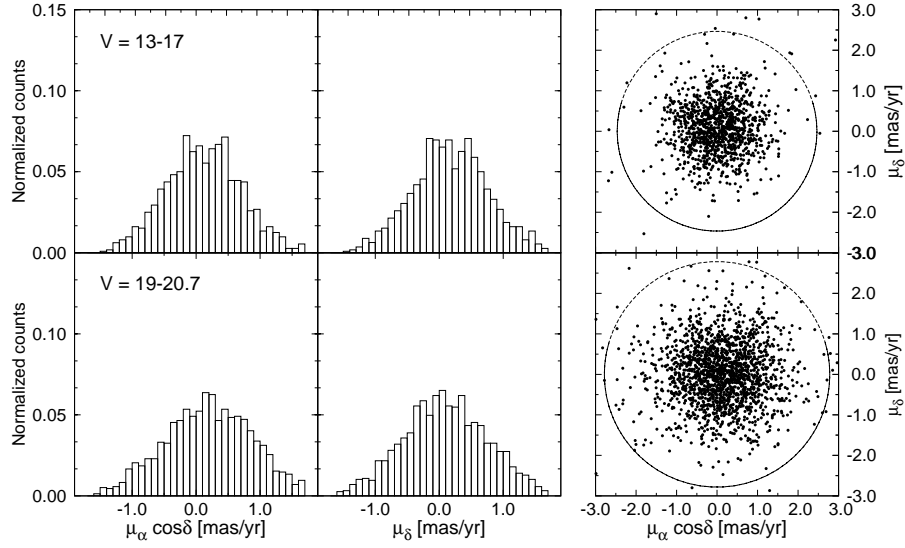
Figure 9: Results for M22. Distributions of $\mu_\alpha \cos\delta$ and μ_δ in bins $V = 13.4 - 17$ and $V = 20 - 21$ mag (left), and the corresponding vector point diagrams (right). The radii of the circles in the right panel are equal to $3S$ with $S = 0.82$ and 0.93 mas yr^{-1} in upper and lower diagram, respectively.
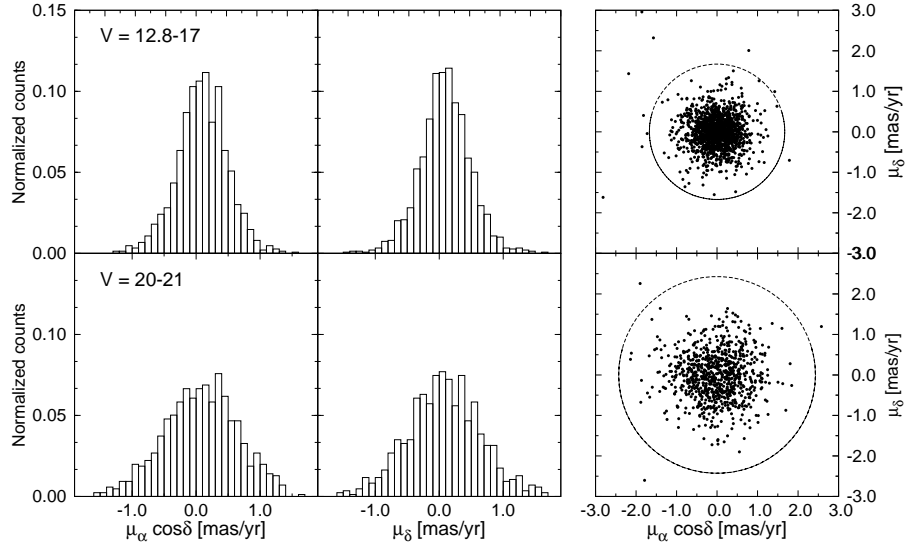

Figure 10: Results for NGC 3201. Distributions of $\mu_\alpha \cos\delta$ and μ_δ in bins $V = 13 - 17$ and $V = 20 - 21$ mag (left), and the corresponding vector point diagrams (right). The radii of the circles in the right panel are equal to $3S$ with $S = 0.45$ and 0.82 mas yr^{-1} in upper and lower diagram, respectively.

Figure 11: Results for NGC 6362. Distributions of $\mu_\alpha \cos\delta$ and μ_δ in bins $V = 13 - 17$ and $V = 20 - 21$ mag (left), and the corresponding vector point diagrams (right). The radii of the circles in the right panel are equal to $3S$ with $S = 0.70$ and 1.54 mas yr^{-1} in upper and lower diagram, respectively.

Figure 12: Results for NGC 6752. Distributions of $\mu_\alpha \cos\delta$ and μ_δ in bins $V = 12.8 - 17$ and $V = 20 - 21$ mag (left), and the corresponding vector point diagrams (right). The radii of the circles in the right panel are equal to $3S$ with $S = 0.56$ and 0.93 mas yr^{-1} in upper and lower diagram, respectively.
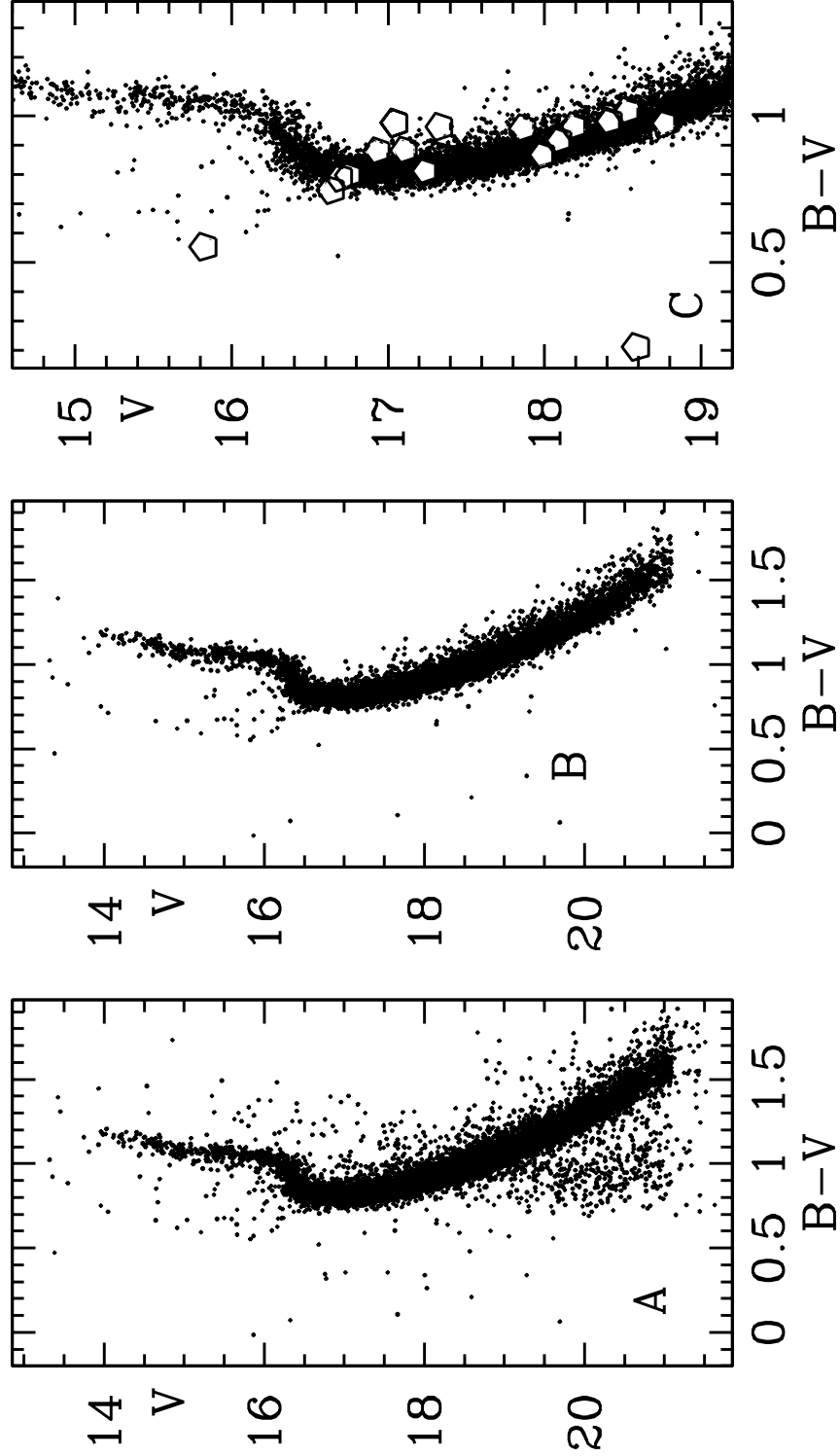
Figure 13: A: CMD of M4 showing all stars with measured relative proper motions and good photometry. B: the same diagram showing likely cluster members only, i.e. stars with $mem = 2$. C: same as B but with marked locations of known variable stars with $mem = 2$.
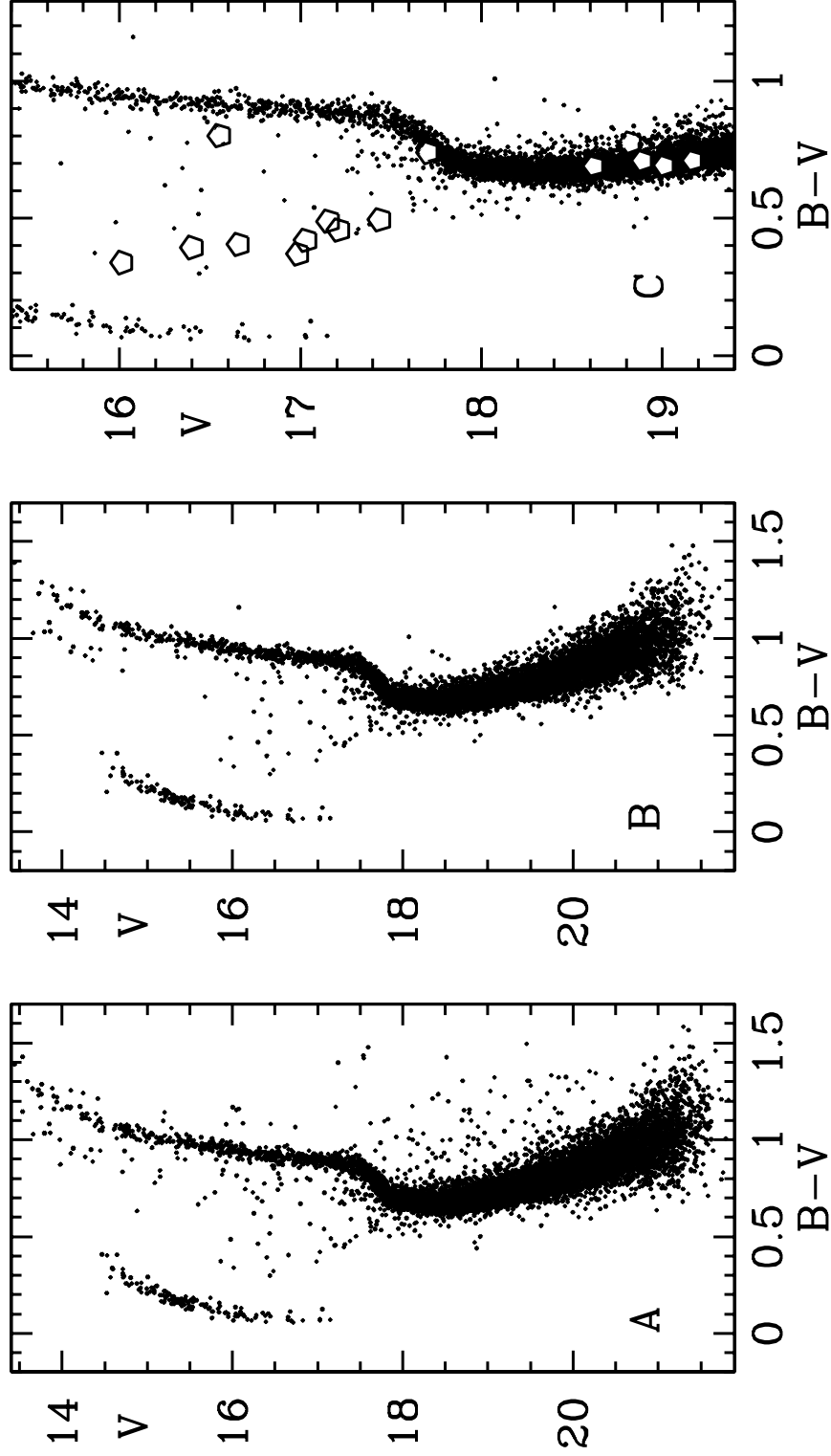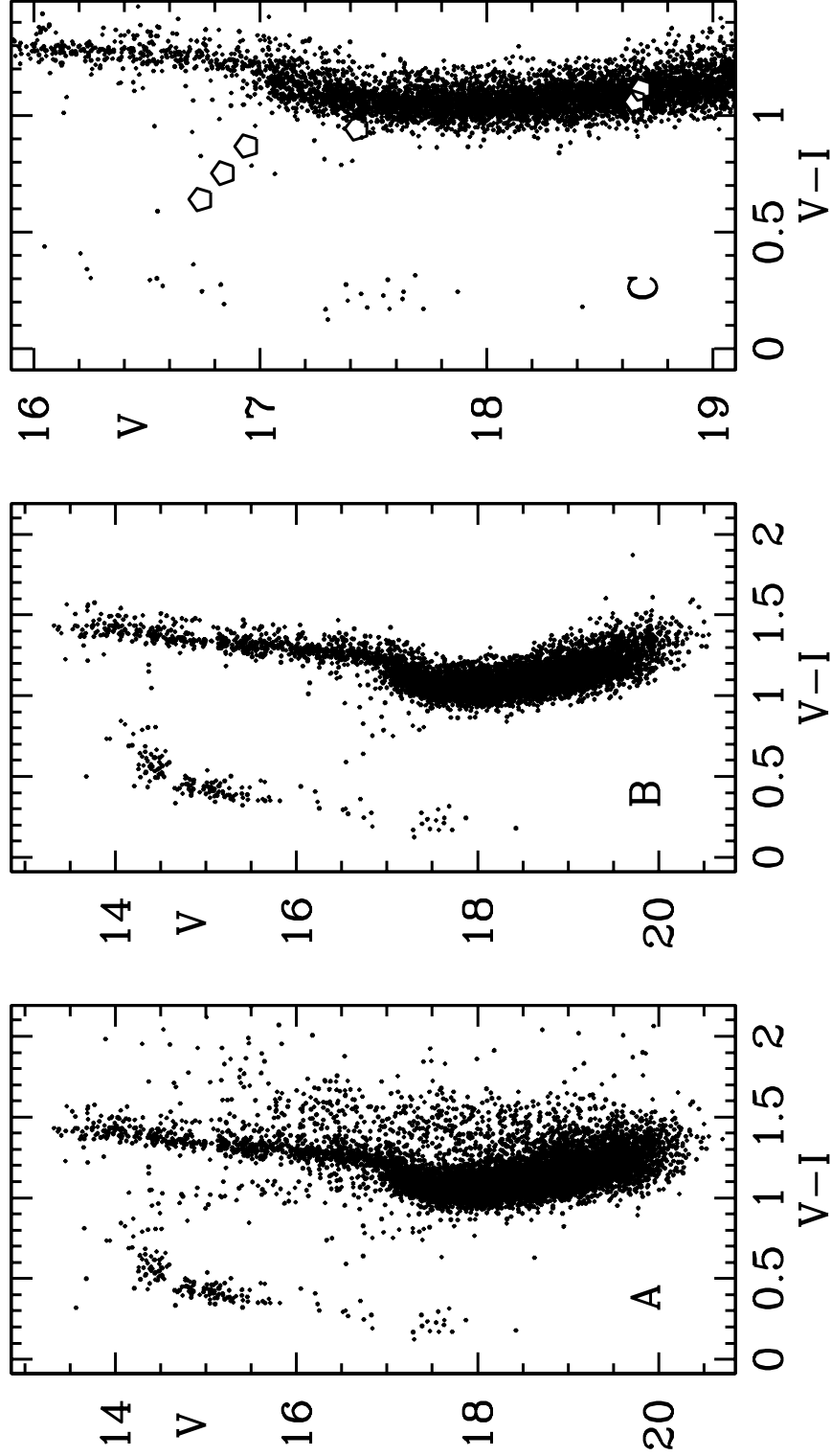
Figure 14: A: CMD of M12 showing all stars with measured relative proper motions. B: the same diagram showing cluster members only, i.e. stars with $mem = 1$ or 2. C: same as B but with marked locations of known variable stars with $mem = 2$.

Figure 15: A: CMD of M22 showing all stars with measured relative proper motions. B: the same diagram showing cluster members only, i.e. stars with $mem = 1$ or 2. C: same as B but with marked locations of known variable stars with $mem = 2$.
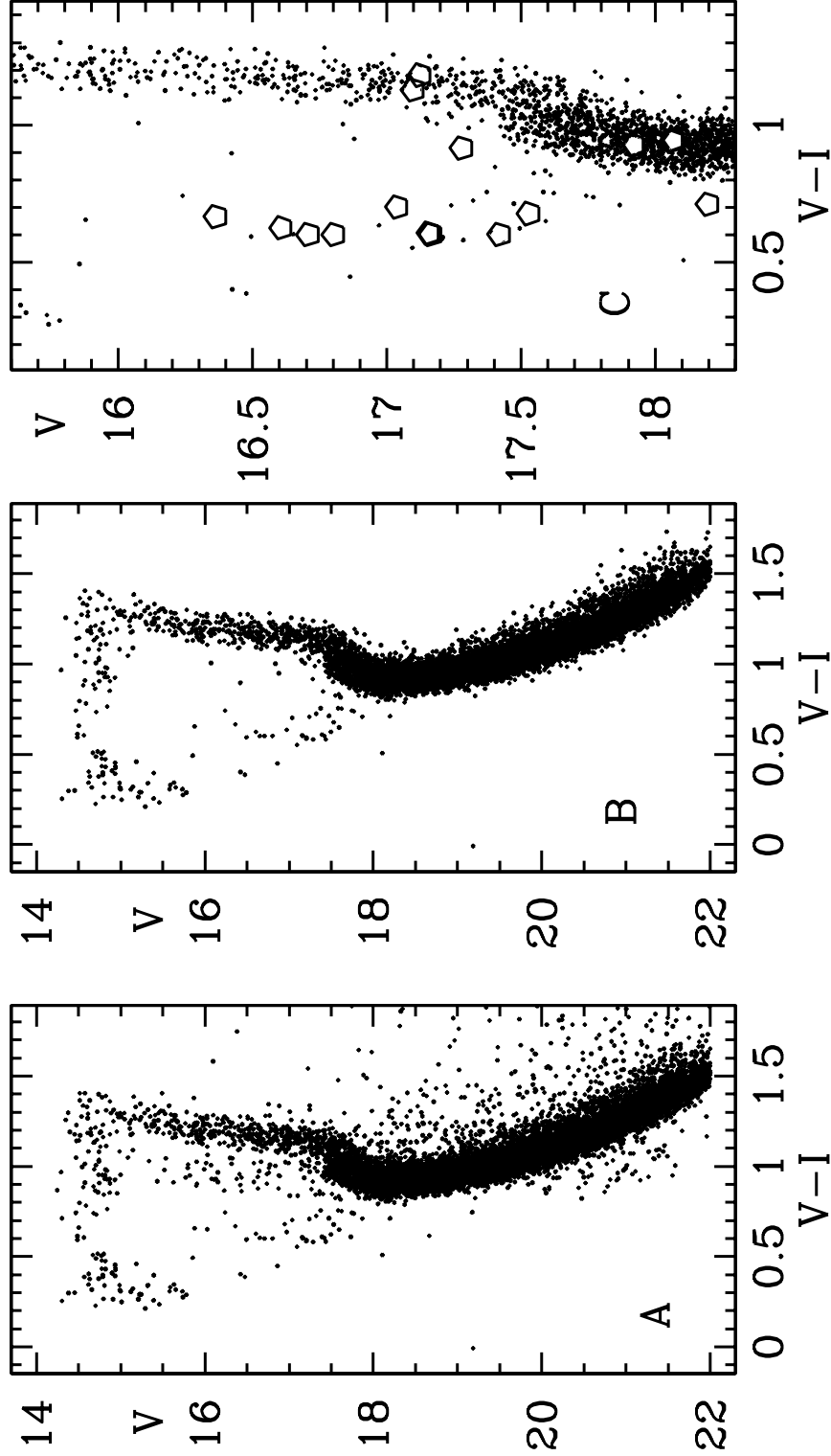
Figure 16: A: CMD of NGC 3201 showing all stars with measured relative proper motions. B: the same diagram showing cluster members only, i.e. stars with $mem = 1$ or 2. C: same as B but with marked locations of known variable stars with $mem = 2$. In order to visualize the horizontal branch, bright stars with poorer photometry were included in this plot.
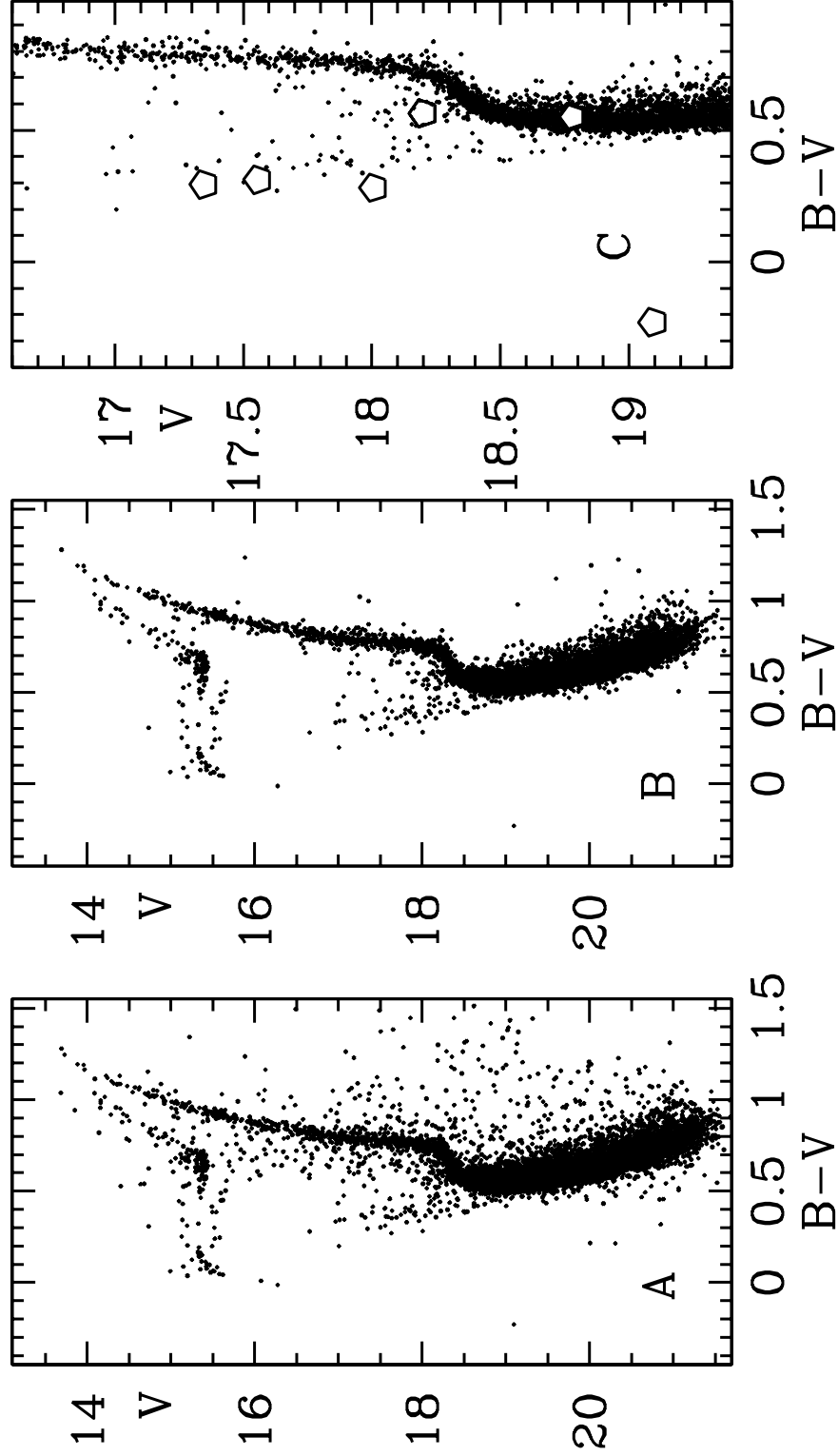
Figure 17: A: CMD of NGC 6362 showing all stars with measured relative proper motions. B: the same diagram showing cluster members only, i.e. stars with *mem* = 1 or 2. C: same as B but with marked locations of known variable stars with *mem* = 2.
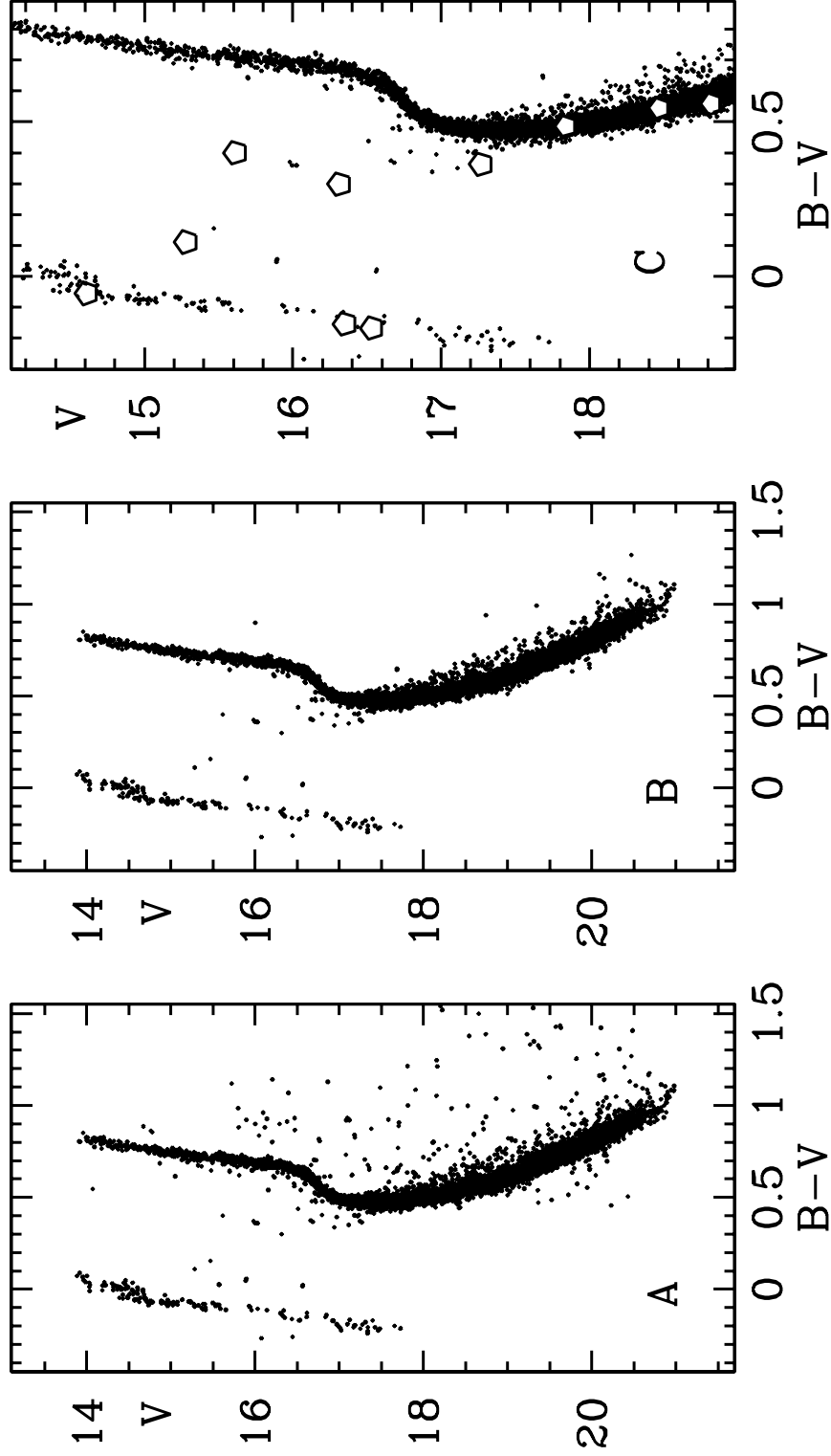
22

Figure 18: A: CMD of NGC 6752 showing all stars with measured relative proper motions. B: the same diagram showing cluster members only, i.e. stars with *mem* = 1 or 2. C: same as B but with marked locations of known variable stars with *mem* = 2.